IASS 2023
July 10–14 Melbourne
Integration of Design and Fabrication

Proceedings of the IASS Annual Symposium 2023
Integration of Design and Fabrication
10–14 July 2023, Melbourne, Australia
Y.M. Xie, J. Burry, T.U. Lee and J. Ma (eds.)

Experimental investigation on the bending response of reuse-ready timber slabs – The Pixel Slab System

Xavier ESTRELLA[*a], Johnny SYRIANI [a], Corentin FIVET [a]

[*] [a] École Polytechnique Fédérale de Lausanne (EPFL), Structural Xploration Lab (SXL)
Passage du Cardinal 13b, 1700 Fribourg, Switzerland
edisson.estrellaarcos@epfl.ch

Abstract

Current construction practices follow linear economic models of "take-make-dispose" that result in substantial material landfilling after the end-of-life of buildings. This issue takes relevance given the construction industry's significant stake in the high levels of resource depletion and waste production observed today. As an attempt to address the problem, this paper presents an experimental investigation on the bending behavior of glue-laminated timber (GLT) slabs -Pixel Slab System- designed for open-ended reuse following Circular Economy principles. The system employs an arrangement of orthogonally intersecting GLT beams to form a reuse-ready grid slab, relying on adjustable static heights, reversible connections, and modular elements to guarantee easy disassembly and reassembly in unknown configurations. To evaluate the system performance, twelve full-scale GLT beams were tested under bending load, employing different spans, depths, and connection placements. Results showed that the system has adequate performance under 3- and 4-point loads; however, the use of notches at the intersections reduced its stiffness and moment capacity by 23% and 29%, respectively. Using reversible steel connections to join consecutive slab modules proved to deliver a proper mechanism to transfer axial, shear, and bending loads, while not affecting the elastic response or failure mode of the beams. Finally, a constructability analysis showed that the concept poses no constraints to on-site construction/deconstruction, since low-tech procedures are used for assembly/disassembly.

Keywords: Component reuse, design for deconstruction, circular economy, sustainable buildings, wooden beams.

1. Introduction

The Pixel Slab is a new slab-column system designed for deconstruction and open-ended reuse over several lifespans. By employing modular elements and reversible connections, the proposed concept allows effortless assembly/disassembly procedures and subsequent reuse in diverse architectural layouts, including ones requiring greater static height [1]. As Figure 1 shows, the system is comprised of modular timber slab elements (2.4×2.4 m) made up of orthogonally intersecting beams that transfer loads to adjacent slabs or columns. Slabs are arranged horizontally by means of in-plane “IP” connections to create a lateral surface. If required by design, the slab’s thickness can be increased by vertically attaching additional slab elements with out-of-plane “OoP” connections to reach longer spans or greater loads. Columns can be placed at any position within the slabs to allow flexible layouts, and their length can vary to satisfy different story heights. This way, the structural elements pose no restrains to flexible architectural requirements, making room for future open-ended reuse. Finally, non-structural elements, such as tiles or insulation, can be assembled on top of the slab elements to provide a flat surface and disassembled for replacement or reuse.

Slab elements are manufactured using glue-laminated timber (GLT) beams with half-lap joints (beam-to-beam "B2B" connectors) at the orthogonal beam intersections, forming a uniform grid across the slab. This allows standardizing the manufacturing by using a single beam geometry for all elements in the modules while being compatible with the current GLT manufacturing process.

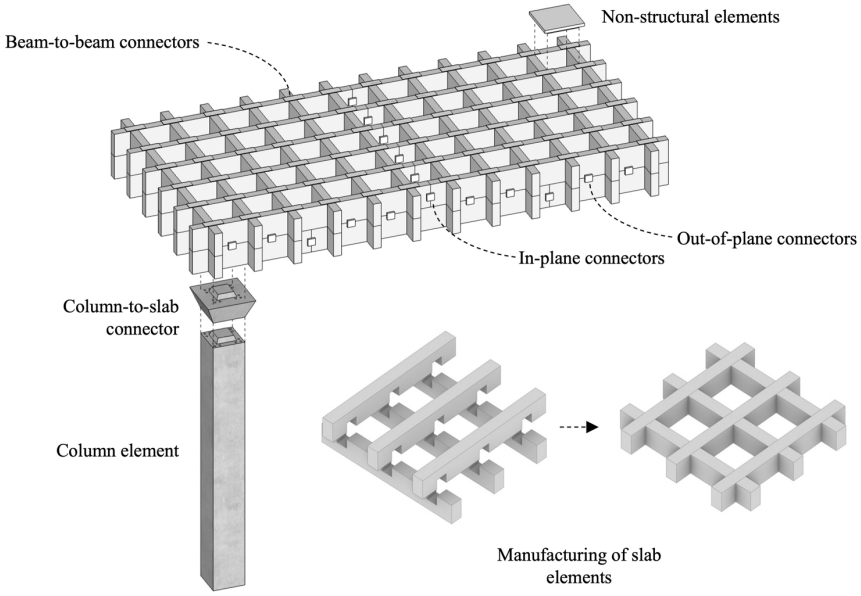

Figure 1. Elements of the Pixel Slab system and manufacturing of slabs.

To better understand the structural performance of the Pixel Slab under vertical loads, this paper presents an experimental investigation on the bending behavior of two main system components: (1) superimposed GLT beams with OoP connectors, and (2) GLT beams with notched B2B connectors. Test results provided insightful information on the load-carrying capacity of the system, geometry/capacity connections compatibility, and suitable design strategies for component design. A full understanding of these phenomena is key for proper implementation of the Pixel Slab, since the slab's behavior, strength, stiffness, and deflection are governed by the mechanical properties of the beams and their connections.

2. Connection design

2.1. Out-of-plane OoP connections

The Knapp MEGANT connector [2] is proposed for the OoP connection. To achieve the composite action between two beams, the connectors need to be placed horizontally at the interface between the top and bottom beams as Figure 2(a) shows. To minimize the impact on the B2B connections, only the smaller Knapp connector length of 310 mm was selected. Three width variants exist for this length, with capacities ranging from 97 to 156 kN and slip modules from 40 to 88 kN/mm. To determine the connection capacities, the MEGANT connector variant was maximized for each cross-section width.

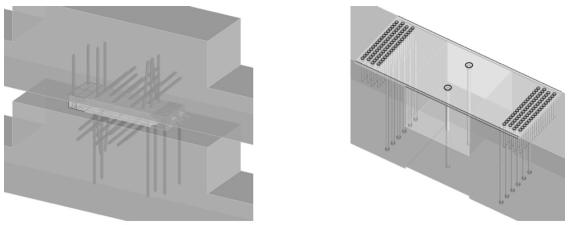

Figure 2. (a) Out-of-plane OoP connection, and (b) beam-to-beam B2B connection.

One drawback of this connection as it is available, is that while it is reversible, it does require to be oriented in the right direction to achieve its highest capacity and slip modulus as provided by the manufacturer. Indeed, in order to benefit from the 45° screws working in withdrawal (tension), they need to be oriented in the direction of the shear force. Alternatively, the screws would work mainly in shear and compression, which are significantly weaker. The load-carrying capacity in this "weak"

orientation is 30-40% that obtained in the "strong" orientation [3]. The slip modulus for the connection in the "weak" orientation is not given in the manufacturer specifications.

To calculate the composite action between elements the gamma-method was used as presented in EN1995.1.1 - Annex B [4]. This method requires the definition of the connection's slip modulus, spacing and element length. For serviceability limit state calculation, the above slip modulus K_{ser} can be used, while for ultimate limit state calculations, a reduced slip modulus $K_u = 0.66\ K_{ser}$ needs to be used as per EN1995.1.1 – 2.2.2 (2) [4]. These are then used to determine gamma coefficients relating to the degree of shear transfer at the interface between two elements. Using these coefficients, the effective bending stiffness $(EI)_{eff}$ can be obtained for direct use in standard calculations. Besides, since all elements have the same rectangular cross-section and modulus of elasticity, the effective height can be calculated as:

$$(EI)_{eff} = E\frac{bh_{eff}^3}{12} \Longrightarrow h_{eff} = \left(\frac{12\cdot(EI)_{eff}}{Eb}\right)^{(1/3)} \quad (1)$$

The results for the obtained effective bending stiffnesses and heights for the considered cross-sections and MEGANT connectors are summarized in Figure 3. Figure 3(a) shows that for two-layer elements, i.e., when two slabs are superimposed, the effective bending stiffness obtained from the gamma-method for the 800 mm connector spacing was 33% of the maximum theoretical stiffness compared to 17% for three-layer elements. This corresponded to effective heights of two-layer elements being on average 69% of the maximum theoretical value compared to 55% for the three-layer elements.

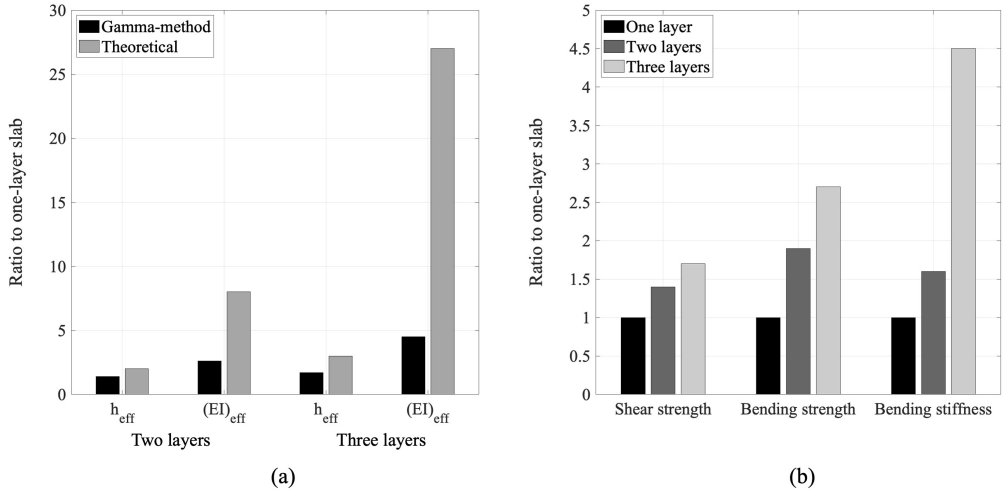

Figure 3. (a) Comparison between theoretical and calculated values for a MEGANT connector spacing of 800 mm, and (b) comparison between strength and stiffness for different element layers.

Compared to single layer elements in Figure 3(b), these gains represent a 38% increase in height for two-layer elements and 65% for three-layer elements. In terms of strength, this would translate to a 38% increase in shear strength and 91% increase in bending strength for two-layer elements. For three-layer elements, those gains would equate to a 65% increase in shear strength and 173% increase in moment resistance. These gains are much lower than the maximum theoretical 2 and 4 times increase in shear and bending strength respectively for the two-layer elements, and 3 to 9 times increase in shear and bending strength respectively for the three layers. In terms of stiffness, the OoP connection results in a 160% and 350% improvement for two- and three-layer elements over the single element layer.

2.2. Beam-to-beam B2B intersection connections

The proposed solution consists in using 90º nails working in shear through a steel plate to transfer the normal forces from the bending moments across the discontinuity. This connection benefits from nails having a smaller diameter and minimum spacings requirements to obtain a significantly higher the

number of fasteners within the limited space available. Here for both tensile and compressive forces, the nails work in shear between the timber beam and the steel plate. The latter then transfers these normal forces across the beam intersection. The steel plate's capacity in tension is defined by the net area, or block shear capacity while its compressive capacity is controlled by the flexural buckling capacity. To this end, fully threaded countersunk head "stability" screws are positioned at the plate centerline to halve the effective length and keep the steel plate as thin as possible. These "stability" screws also serve a fabrication purpose in tying the intersection beam together. Here, again, the connection configuration has the normal force transmitted at the top fiber of the cross-section resulting in an equivalent moment resistance of $M_{Rd} = 5Nh / 6$.

Regarding the shear strength, it is defined by the minimum of the shear capacity of half of the beam cross-section, or the augmented capacity obtained using the reinforcement screws on both sides of the joint. The B2B connection is illustrated in Figure 2(b).

3. Experimental testing

3.1. Out-of-Plane OoP connections

Three-point bending tests were carried out to investigate the capacity of the double beams assembled using the OoP connectors. In total, five tests were conducted: for the first three tests (OoP1, OoP2 and OoP3) the double beams were linked using two MEGANT connectors spaced at 2300 mm, while for the last two tests (OoP4 and OoP5) the beams used six MEGANT connectors spaced at 767 mm along the beams. The specimens were two 4800 mm long GLT elements with a cross-section of 180×280 mm and a GL24h strength class. For the connections, two or six Knapp MEGANT 310×100×40 mm were used. Each connection consists of two connector plates, two clamping jaws, 4–8×240 mm fully threaded screws, 26–8×160 mm fully threaded screws and 2–16×340 mm threaded rods with washers and nuts.

The testing setup is shown in Figure 4. To prevent crushing perpendicular to the grain at the supports, 180×300×5 mm steel plates were screwed on the underside of the bottom GLT beam. At the load application point, located at midspan, the jack head area of 180×300 mm was sufficiently large to avoid crushing perpendicular to grain for the given load and no bearing plate was added. Deformations were recorded at several locations in the beams employing linear variable differential transformers LVDTs.

The testing procedure was divided in two parts. The first part consisted of three loading cycles up to 10 kN and down to 1 kN with a two-minute interval between each cycle. The results from the last two loading cycles were used to determine the effective elastic bending stiffness $(EI)_{eff}$ of the specimens. The obtained elastic bending stiffness can then be used to calculate the effective height of the composite cross-section, as shown previously. The second part consisted in loading the specimen until failure. The loading rate was set to 0.02 mm/s (1.2 mm/min) for both parts of the test.

Figure 4. Three-point testing setup for OoP specimens and failure modes.

The elastic bending stiffness was computed for all specimens from the results of the first part of the test. For the specimens OoP1-2-3, the average effective bending stiffness was of $(EI)_{eff,avg}$ = 6.93e12 N/mm^2 with a coefficient of variation (CoV) of 19.1%. This high CoV value is explained by the higher performance observed for specimen OoP3. The obtained effective bending stiffness translates an average effective height of $h_{eff,avg}$ = 432 mm, assuming the mean elastic modulus E = 11 500 N/mm^2. This is below the theoretical values obtained using the gamma-method, for both serviceability and ultimate limit states. In addition, this average effective height is lower than the theoretical value for two vertically stacked beams having no shear transfer between them. Superimposing two beams would result in doubling the stiffness which result in an effective height equal to $h_{2,eff} = 2^{1/3} \cdot h$ = 353 mm Therefore, the large 2300 mm connector spacing shows an effective reduction in overall bending stiffness of the system. This could, however, not entirely be caused by the presence of the connectors and may be also explained by the elastic modulus of specimens OoP1 and OoP2 being lower than the mean value due to the high natural variability of timber elements. Another possible explanation for such observation could relate to the fact that the ends of the top beam, past the connection point, do not contribute to the overall stiffness of the system. Indeed, since all the internal forces are transferred at the connector point, only the central half of the top beam is being solicited.

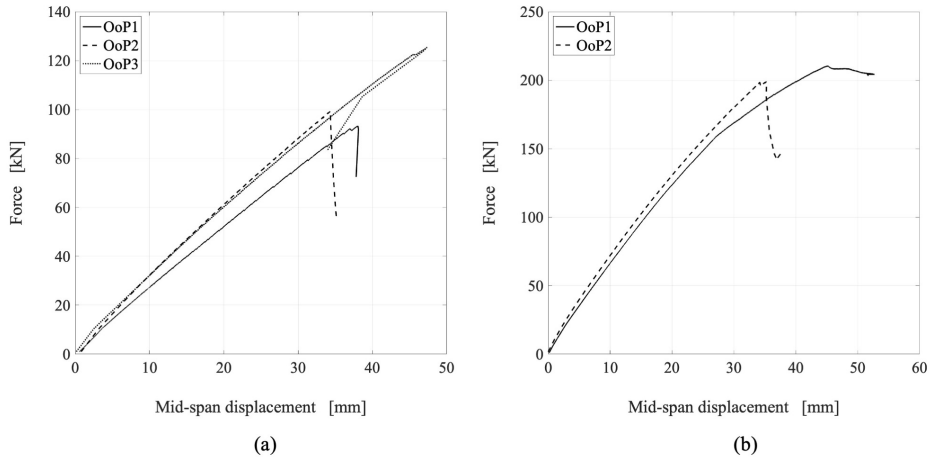

Figure 5. Force-displacement results for OoP specimens.

For the second part of the test, the specimens were loaded up to failure. From the force-displacement results in Figure 5, it can be observed that for specimens OoP1-2-3 there was a higher initial stiffness which reduced slightly around a midpoint deflection of 4-5 mm and remained constant throughout the test. All three specimen exhibited a linear elastic behaviour up to failure. Specimen OoP1 showed the lowest stiffness and ultimate load of 93.3 kN. Specimens OoP2 and OoP3 showed a very similar stiffness throughout the test, however the specimen OoP2 failed at a load of 99.3 kN compared to 125.3 kN for specimen OoP3. The failure mechanism was the same for the three specimens with the bottom beam failing on the underside due to tension from the bending stresses (Figure 4). In all three cases the tension crack originated at a knot on the bottom lamella which then propagated across the cross-section. This failure mode was extremely brittle as can be observed in the graphs by the instantaneous drop in force following the ultimate load.

For specimens OoP4 and OoP5, the latter can be seen to have a higher stiffness overall. For both specimens however, the force-displacement relationship is not as linear as for the specimens OoP1-2-3. After reaching 165 kN, a decrease in stiffness can be observed, which is more apparent in OoP4. This can be due to cracks forming in the beams as the loading increases. However, the post-peak behaviour of specimen OoP4 was not representative since towards the end of the test, the steel bearing plates at the supports yielded, resulting in crushing of the bottom beam at the supports. This therefore limited the beam develop additional bending stress and the specimen simply exhibited larger support settlement before the test was stopped. Nonetheless, both specimens reached a peak load around 200 kN which is

roughly twice that of specimens OoP1-2-3, while exhibiting similar midpoint deflections. For both specimens OoP4 and OoP5, the failure mechanism was the same with the bottom beam reaching its tension capacity on the bottom lamella due to bending.

A similar strength performance was observed for specimens OoP1 and OoP2 with peak bending moments around 110 kN-m. Specimen OoP3 on the other hand, again exhibited a higher performance reaching a maximum bending moment of 144.1 kN-m. This leads to an average bending resistance of 121.9 kN-m and translates to a CoV of 16.1% for these three specimens. With regards to mid-span deflection, the average for specimens OoP1-2-3 was 39.9 mm, with a CoV of 16.8%. The high CoV values here are due to the relatively high performance of specimen OoP3. In the second series of tests, specimens OoP4 and OoP5 performed very similarly with an average ultimate bending moment of 235.1 kN-m and a CoV of 4.0%. With regards to maximum mid-span deflection, the resulting average deflection was found to be 40.2 mm for a CoV of 17.5%. This high CoV value can be attributed to the bearing plate failure for specimen OoP4, as discussed previously.

3.2. Beam-to-beam B2B intersection connections

Four-point bending tests were carried out to investigate the capacity of the B2B connection. In total, seven tests were conducted: the first test was done on a reference beam with no notches or connection (Ref), then three tests had the connection on the tension side of the beams (T1, T2, T3) while the last three tests had the connection on the compression side of the beams (C1, C2, C3). The specimens were made using 2400 mm long GLT elements of cross-section 180×280 mm and strength class GL24h. The specimens T1-2-3 and C1-2-3 had two notches of dimension 180×180×140 mm located at 300 mm on each side of the beam centerline. Those notches were filled using GLT blocks of the same dimension as the notches and were oriented with the grain perpendicular to the beam direction to replicate the intersecting beam. The connections consisted of 180×480×6 mm steel plates of grade S355, fastened using 66–6 mm diameter × 100 mm long LBA nails, and 2–9 mm diameter – 260 mm long fully threaded countersunk-head VGS screws. The shear reinforcement screws used 6–7 mm diameter – 260 mm long fully threaded cylindrical head screws per side of the notches, for a total of 24 screws per specimen.

Figures 6 and 7 show the testing setups for specimens C and T, respectively. As for OoP specimens, steel plates were installed at the edges to prevent crushing of the wood. Similarly, the testing procedure was divided in two parts. The first part consisted of three loading cycles up to 10 kN and down to 1 kN at each jack. A two-minute pause was made between each cycle. The results from the last two loading cycles were used to determine the effective elastic ending stiffness. The second part consisted of loading the specimen until failure. The loading rate was set to 0.02 mm/s (1.2 mm/min) for both parts of the test.

Figure 6. Three-point testing setup for C specimens and failure modes.

The elastic bending stiffness was computed for all B2B specimens. For the reference specimen this value is a characteristic property since the geometric properties of the element are uniform over its length. On the other hand, for the specimens with the half-lap notches, these obtained values represent effective properties. The effective nature of the obtained bending stiffness can be attributed to the elastic modulus E_{eef} or to the moment of inertia I_{eff}. Therefore, two alternatives were evaluated.

First, the effective elastic modulus E_{eef} was determined considering the full height of the beam h = 280 mm in the calculation of the moment of inertia $I = b \cdot h^3/12$. It was found that for the specimens with the B2B connection in tension and in compression, the obtained values are between 33% and 45% the theoretical mean value of $E_{0,mean}$ = 11 500 N/mm^2 from the GL24h material properties. Comparatively, the reference beam had a 44% higher stiffness compared to the expected mean value. However, it is important to note that since only one reference beam was used in the testing, no statistical relevance can be derived from the obtained results. Alternatively, for the notched specimens, the effective height h_{eff} can be calculated from the effective moment of inertia assuming the theoretical mean modulus of elasticity. These results show, the effective height was lower than the actual beam height by 23% to 31%. Therefore, the notches in the beams have a negative impact the bending stiffness.

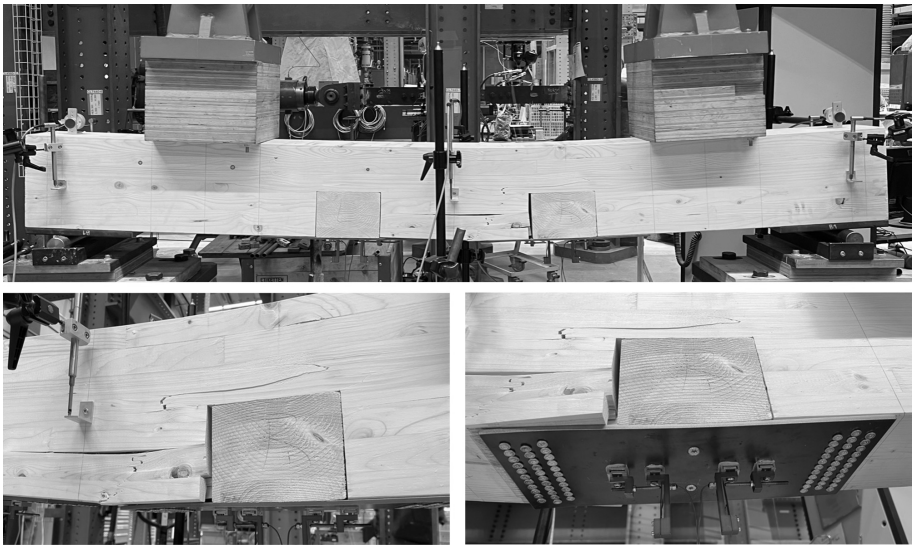

Figure 7. Three-point testing setup for T specimens and failure modes.

As Figure 8(a) shows, the three specimens C1, C2 and C3 exhibited different force-displacement relationships. First, the ultimate load for the specimens C2 and C3 was just above 80 kN while specimen C1 reached 50% higher load at 126.6 kN. This can be attributed to the fact that the failure occurred in the tension fibers between the lines of reinforcement screws in specimen C1. Comparatively, the failure line in specimens C2 and C3 occurred at the shear reinforcement screw location (Figure 6). This discontinuity in the bottom fibers due to the presence of the screws could have resulted in the creation of weaker lines across the width of the beam having a reduced net section to resist the tension force. Therefore, the different failure line could be partly responsible for the observed difference in strength between the specimens. Furthermore, the failure mode of specimens C1 and C3 can be observed to be more ductile.

These specimens show a marked stiffness reduction after reaching around a load 90 kN and 70 kN respectively. From the force-displacement graph, it can be observed that these specimens exhibited sudden strength drops due to crack formation inside the cross-section as the loading increased which reduced the element stiffness. On the other hand, specimen C2 failed in a more brittle manner immediately after reaching its ultimate load. Nonetheless, all three specimens showed a very similar stiffness throughout the testing up to failure and a linear elastic behaviour until cracking occurred.

For specimens T1-2-3, as shown in Figure 8(b), it can be observed that there was a relatively large difference in stiffness between the three specimens up to the onset of the first crack. Following cracking of the beams, failure did not occur immediately. Rather, the specimens exhibited relatively high levels of ductility, especially compared to specimens C1-2-3 as can be observed in Figure 8. The specimens were able to maintain some load-carrying capacity, albeit a very low, or null stiffness, by continuing to deform under constant or slightly increasing load by up to 47 mm for specimen T1 before reaching ruin. This ductility can be attributed to the B2B connections which, due to the shearing of nails-timber interface, resulted in an initial local splitting without the fibers reaching their capacity (Figure 7).

The nailed connection still had load carrying capacity due to the high number of nails in the connection, providing a high degree of redundancy thus translating to the observed ductility. Then, once the deformation reaches a critical point the ruin occurs by the crack propagating perpendicular to the grain. Furthermore, the ultimate load reached by the three specimens was between 70 kN and 80 kN, showing less variability compared to the specimens C1-2-3.

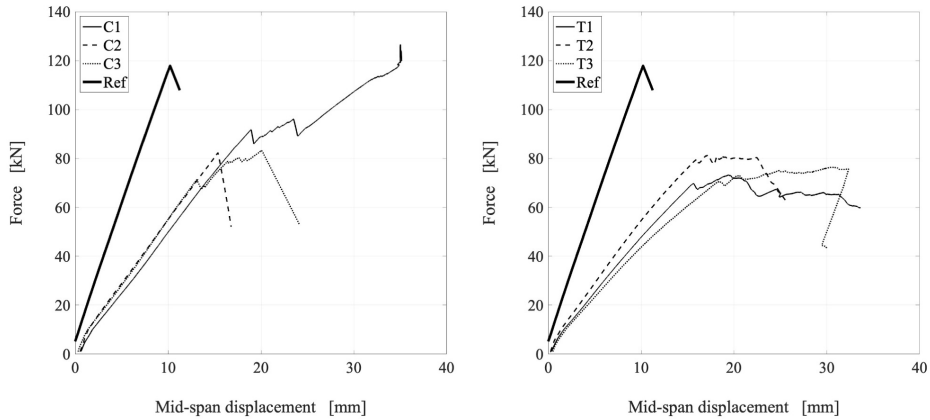

Figure 8. Force-displacement results for B2B specimens.

The reference beam exhibited a linear elastic behaviour throughout the test. The higher stiffness of the beam is apparent in the steeper slope of the force-displacement relationship presented in Figure 8. The failure occurred at the bottom fiber due to the tension stress from the bending moment. While the specimen reached a high ultimate of load, at 117.9 kN, its displacement capacity was limited by the brittle nature of the failure mechanism.

The results for the maximum bending moment and associated jack load and mid-span deflection were computed for all beams from the test data. With regards to the maximum bending moment, all the specimens fitted with the B2B connection reached a similar value around 30 kN-m with the exception of specimen C1 which exhibited a significantly higher performance attaining a bending moment of 50.6 kN-m. This discrepancy leads to a high CoV of 26.0% for the maximum bending moment for specimens C1-2-3. In comparison, specimens T1-2-3 all performed similarly in this regard and displayed a CoV of 5.3%. The reference specimen reached a peak bending moment of 47.2 k-Nm.

For the peak mid-span deflection, the average for specimens C1-2-3 was of 25.4 mm while for T1-2-3 was 33.2 mm, which represents a 31.0% increase compared to specimens C1-2-3. Both series of tests exhibited high variability and dispersion around the mean with a CoV of 36.4% and 24.3% for specimens C1-2-3 and T1-2-3, respectively. For the former, this value can be explained in part by the high performance of specimen C1. For the latter, since in all three tests the maximum bending moment was reached during the plateau region of the force-displacement, the corresponding mid-span deflection values varied according to the propagation of cracks cause by the nail-timber shear failure. This ductile behaviour also explains the higher average for those specimens, which deformed more significantly before reaching their peak capacity.

4. Performance review and design implications

4.1. Out-of-Plane OoP connections

The initial stiffness results show that the gamma-method can be suitable to estimate the effective composite cross-section properties but only at smaller spacings. Indeed, in the first tested configuration with two connectors spaced at 2300 mm, the internal force transfer between the two beams relies solely on those two discrete points. This, in turn, limits the contribution of the top beam since only the central portion of the beam between the two connectors is utilized. In comparison, the second configuration has six connectors evenly distributed along the lengths at one third the spacing of the first configuration. This allows the two beams to be utilized over a longer length and benefits from three times the number of points of force transfer thus distributing the internal forces more gradually along the element length.

Overall, these tests demonstrate that for the OoP connection system to work well for a connector spacing equal to the beam grid spacing, 800 mm or less, corresponding to the second tested configuration. Comparatively, the first configuration with the connector spacing of 2300 mm, would be equivalent to having one connector per beam grid module. This would therefore not be sufficient as the resulting stiffness gains are insufficient to justify the addition of an out-of-plane module.

Therefore, while not achieving a completely rigid connection between the elements, the system can be calculated and analysed easily using the gamma-method. Combined with the reversible nature of the connection, this improved performance compared to the current design of this connection, as presented in Section 2.1, and validated by the testing, and easily implementable calculation methodology makes the Knapp MEGANT connector a viable option for the OoP connection.

4.2. Beam-to-beam B2B intersection connections

A comparison can be made to the expected theoretical failure mechanisms and maximum loads. The unfactored bending capacity of a full 180×280 mm GLT beam is $M_{y,Rd}$ = 60.9 kN-m, which under a 4-point bending setup, should have been reached for a jack load of P = 152.2 kN. For specimens C1, C2 and C3, the expected failure mechanism was the plate buckling under the compression due to bending. The calculated buckling capacity of the 6 mm steel plate was $N_{b,Rd}$ = 120,1 kN, which would have been reached for a bending moment equal to $M_{y,C,Ed}$ = 28.0 kN-m corresponding to a jack load of PC = 70.0 kN. However, those specimens all failed in tension on the underside due to the bending moment (Figure 6). A few reasons can explain this discrepancy.

The first being the potential weakening of the cross-section on the bottom fiber due to the reinforcement screws as discussed previously. The second reason could be the reduced bending stiffness (or corresponding effective cross-section height), which reduced the bending strength of the beams. Indeed, the unfactored bending capacity of a beam of dimensions 180×206 mm – corresponding to the average of the effective heights from specimens C-1-2-3 – can be calculated to be $M_{y,Rd,C,eff}$ = 33.6 kN-m, corresponding to a jack load of $P_{C,eff}$ = 84.0 kN. This effective capacity is, however, still higher than the expected failure load for buckling of the steel plate. Therefore, in addition to the B2B connection, another compression force transfer mechanism must be involved around the notch, since the B2B connection did not reach its expected buckling capacity.

Indeed, upon reaching higher curvature and slip in the connection due to the increased beam deformation and bending force respectively, the notch and transverse beam "block" were seen to be in contact. The compressive stresses could therefore be transferred by compression perpendicular to grain between those elements. This would explain the observed failure mechanism in bending and the ultimate loads around 80 kN for specimens C2 and C3 corresponding to the effective strength of the element. For specimen C1, the failure load corresponds to that of the reference beam which failed at about 80% of the expected jack load. This could be explained by variability in the timber beams with the presence of knots on the bottom fiber where the failure occurred in specimen C1, or by the high stiffness of the tested reference beam.

For specimens T1, T2 and T3, the failure mechanism was expected to be the shear failure of the nail-timber connection, with a capacity of V_{Rd} = 174.2 kN, which would be reached for a bending moment equal to $M_{y,T,Ed}$ = 40.7 kN-m at a jack load of P_T = 101.7 kN. This failure mode corresponds to the observations from the testing as Figure 7 shows. In all three cases, the failure initiated from a lengthwise splitting of the cross-section at the edge nail locations closest to the notch, which then propagated across the cross-section. This can be due to the shear capacity of the beam being reached at this point. However, the failure load only reached 70 to 80% of the expected value. This could again be due to the reduced stiffness of the beams, as discussed above. Using the average h_{eff} = 203 mm for the three specimens, the equivalent bending moment required to develop the connection's shear capacity V_{Rd} = 174.2 kN can be calculated as $M_{y,Rd,T,eff}$ = 29.5 kN-m. This bending moment is reached at a jack load $P_{T,eff}$ = 73.8 kN. For these specimens, calculating the unfactored effective bending capacity using the average h_{eff} results in $M_{y,Rd,eff}$ = 32.6 kN-m. Thus, the beam's effective moment capacity is higher than the equivalent effective connector's moment resistance and relates to the observed failure mode of the nail-timber connection.

4. Conclusions

This paper presents the results of an experimental investigation on the bending behavior of reusable timber slabs – The Pixel Slab System. Twelve beam specimens with different spans, depths, and connections were tested with 3- and 4-point bending setups. Two connection methods were studied: (1) superimposed GLT beams with OoP connectors, and (2) GLT beams with notched B2B connectors.

The proposed OoP connection employed a Knapp MEGANT connector at the interface between the vertically arranged beams. Test results of this connection show that the wider connector spacing did not successfully achieve full composite action between two beams. The smaller spacing however, exceeded the theoretical expectations with regard to the effective heights obtained with the gamma-method. While not achieving full shear transfer between two beams due to the connection slippage, the performance still was found suitable for the application thanks to the reversibility potential of the Knapp MEGANT connector. Yet, the connector's directionality and constructability constraints could be further refined.

The proposed B2B connection uses half-lap geometry to join the intersecting beams together. To achieve the element continuity, a nailed plate is installed on one side of the beams to tie the discontinuous beam ends around the half-lap notch. The results from the experimental testing for this connection shows a significant reduction in stiffness up to 66% of the expected mean value, due to the half-lap notches and the connection slip. In tension, the B2B connection performed as expected. However, in compression, the connection slip induced bearing perpendicular to the grain between the notched ends and the perpendicular block. Hence, care should be taken to dimension the notch to account for this issue.

Acknowledgements

This research was partially funded by the EPFL - ENAC Innovation Seed Grants 2022 program. The steel connectors employed in this research for the OoP tests were facilitated by KNAPP GmbH.

References

[1] A. Muresan, J. Brütting, J. Cañada, D. Redaelli, and C. Fivet, "Design Space of Modular Slab Systems with Discrete Stiffness Distribution and Irregular Column Layout," in *Proceedings of the IASS Symposium 2018*, Boston, USA, 2018.

[2] Knapp-Verbinder, "MEGANT (R) - heavy duty system | Knapp Connectors," *[Online]. https://www.knapp-verbinder.com/en/produkt/megant-heavy-duty-system/?v=11486*, 2021.

[3] Austrian Institute of Construction Engineering, "European Technical Assessment ETA-15/0667 of 22.07.2019," Austrian Institute of Construction Engineering, 2019.

[4] European Committee for Standardization, "Eurocode 5: Design of timber structures - Part 1-1: Common rules and rules for buildings," European Committee for Standardization, 2004.